Journal of Magnetic Resonance 195 (2008) 9–16

Contents lists available at ScienceDirect

Journal of Magnetic Resonance

journal homepage: www.elsevier.com/locate/jmr

Sensitivity losses and line shape modifications due to molecular diffusion in continuous encoding ultrafast 2D NMR experiments

Patrick Giraudeau *, Serge Akoka

Université de Nantes, CNRS, Chimie et Interdisciplinarité: Synthèse, Analyse, Modélisation (CEISAM), UMR 6230, Faculté des Sciences, B.P. 92208, 2 rue de la Houssinière, F-44322 Nantes Cedex 03, France

ARTICLE INFO

Article history:
Received 26 May 2008
Revised 5 August 2008
Available online 9 August 2008

Keywords:
Ultrafast 2D NMR
Molecular diffusion
Sensitivity
Resolution
Multi-echo encoding

ABSTRACT

Recent ultrafast techniques make it possible to obtain multidimensional (nD) NMR spectra in a single scan. These ultrafast methods rely on a spatial encoding process based on radiofrequency (RF) pulses applied simultaneously with magnetic field gradients. Numerous approaches have been proposed in the past few years to perform this excitation process, most of them relying on a continuous excitation of the spins throughout the whole sample. However, the resolution and sensitivity of ultrafast nD spectra are often reduced by molecular diffusion effects due to the presence of gradients during the excitation process. In particular, increasing the excitation period is necessary to improve the resolution in the ultrafast dimension, but it leads to high sensitivity losses due to diffusion. In order to understand better and to limit molecular diffusion effects, a detailed theoretical and experimental study of the various continuous ultrafast excitation processes is carried out in the present study. New numerical simulations of ultrafast echo line shapes are presented and compared to experimental data. The evolution of the signal intensity with the excitation process duration is also simulated and compared to experimental intensity losses. The different excitation schemes are compared in order to determine the best excitation conditions to perform 2D ultrafast experiments with optimum resolution and sensitivity. The experimental and theoretical results put in evidence the efficiency of the multi-echo scheme.

© 2008 Elsevier Inc. All rights reserved.

1. Introduction

Nuclear magnetic resonance (NMR) is a powerful analytical tool used in a wide range of applications, from the study of chemical structures and dynamics to pharmaceutical and medical applications. In particular, multidimensional (nD) spectroscopy [1,2] plays a central role among NMR techniques, as it brings a resolution enhancement that is essential to elucidate complex molecular structures. However, the length of the experiments (several hours)—necessary to complete the acquisition of an nD FID—often hampers the implementation of nD spectra. This is a consequence of the nD acquisition process, which relies on the repetition of numerous transients with incremented delays. Beyond the timetable constraints caused by the subsequent experiment duration, this incrementation procedure makes nD NMR very sensitive to temporal instabilities, leading in particular to large noise ridges along t_1 dimension [3]. Moreover, it makes nD NMR unsuitable for the study of short timescale phenomena.

Numerous approaches have been proposed to overcome this time limit and to obtain 2D NMR spectra in a reduced time. Schanda and Brutscher [4] proposed an optimization of delays and pulse angles in the HMQC sequence (SOFAST-HMQC), leading to 2D spectra of protein samples in a few seconds. However, this approach still relies on the incremented acquisition scheme described above. Several strategies were considered to bypass this difficulty. The application of linear prediction (LP) [5,6], maximum entropy (MaxEnt) [6,7] or projection–reconstruction (PR) [8] methods to 2D NMR was proposed, based on the acquisition of a small number of t_1 increments. An appropriate algorithm was then applied to calculate the whole 2D FID $s(t_1, t_2)$. Alternative strategies to Fourier transform (FT) NMR were also suggested, such as FDM (filter diagonalization method) [9] or covariance NMR. Kupce and Freeman developed another non-FT method called Hadamard spectroscopy [10,11], based on a frequency-domain excitation, which found interesting applications in biomolecular NMR [12]. The aforementioned strategies permit an efficient limitation of the indirect domain sampling duration; however, all of them require the repetition of several transients. Therefore, the experiment duration is often limited by the relaxation delay, and several seconds are necessary to obtain a 2D spectrum.

A totally different approach was recently proposed by Pr. Frydman and co-workers [13,14], allowing the acquisition of 2D NMR spectra within a single scan. In this "ultrafast 2D NMR"

* Corresponding author. Fax: +33(0)2 51 12 57 12.
E-mail address: patrick.giraudeau@univ-nantes.fr (P. Giraudeau).

1090-7807/$ - see front matter © 2008 Elsevier Inc. All rights reserved.
doi:10.1016/j.jmr.2008.08.001

method, the usual t_1 encoding is replaced by a spatial encoding, and after a conventional mixing period, the spatially encoded information is decoded by a detection block based on echo planar imaging (EPI) [15]. The spatial encoding scheme initially proposed [13,14] relies on a succession of selective pulses applied during alternating bipolar gradient pairs. It suffers from several drawbacks as it requires fast gradient switching carefully synchronized with RF irradiation. Moreover, it leads to the appearance of undesirable "ghost peaks" [16] in the indirect domain. Consequently, this discrete excitation scheme was replaced in the past few years by several continuous encoding patterns [17–22] relying on the combination of continuously frequency-swept pulses applied during a bipolar gradient.

These different alternatives to discrete excitation were recently described by Shrot and Frydman [20]. However, this study was limited to a theoretical description of spin phase evolutions which did not take into account the various sensitivity loss sources. Consequently, it seems indispensable to proceed to a detailed study of the various encoding patterns available in order to determine the excitation conditions leading to optimum resolution and sensitivity. In particular, resolution along the ultrafast domain is a key factor for improving the quality of ultrafast nD spectra. We have recently shown [17] that this resolution was directly proportional to the average time T_e spent by magnetizations in the transverse plane. This duration is directly related to the spatio-temporal encoding constant C, which is the $\Omega_1 \cdot z$ dependence of the phase evolution at the end of the encoding process. As a consequence, improving ultrafast resolution requires increasing the duration of the spatial encoding process. However, increasing T_e is limited by various factors. The first limitation comes from spectral width considerations. When T_e increases, the acquisition duration T_a must be increased as well to observe all relevant peaks in the ultrafast dimension. Unfortunately, the spectral width in the conventional dimension is inversely proportional to T_a. Therefore, increasing T_e leads to a limited spectral width in the conventional domain. However, high T_e values can still be convenient to observe reduced spectral windows (for example in the case of J-resolved spectroscopy [23]). High T_e values can also lead to signal losses due to transverse relaxation, when T_2 is not negligible compared to T_e. Finally, signal losses due to molecular diffusion effects in the presence of magnetic field gradients can be observed. These effects may cause important signal losses and line shape distortions at high T_e values.

In a recent paper [24], we showed that diffusion was the most constraining of the above factors. A detailed description of diffusion effects in ultrafast experiments was given very recently by Shrot and Frydman [25]. The authors developed a very complete theoretical model to determine diffusion losses throughout the sample. Analytical diffusion loss profiles were compared to numerical simulations and to experimental observations for three excitation schemes. A very good adequacy was obtained between simulated, experimental and theoretical data, but this study was performed for small T_e values only, for which diffusion effects are not a major obstacle. The influence of T_e on the compromise between resolution and sensitivity was not discussed in details in this paper. And, to our knowledge, the influence of diffusion effects on ultrafast echo line shapes was never described.

Consequently, a comparison of the different continuous excitation schemes for various T_e values is necessary to determine their relative dependence on diffusion effects. In the present paper, a general theoretical and experimental study of diffusion losses for each continuous excitation scheme is carried out. New echo line shape numerical simulations are presented and compared to experimental results in order to find the best excitation conditions to perform 2D ultrafast experiments with optimum resolution and sensitivity.

2. Theory

2.1. Description of continuous encoding schemes

The main continuous excitation schemes are described in Fig. 1. The two first ones (Fig. 1A and B) achieve an amplitude-modulated encoding, whereas the schemes on the second line (Fig. 1C–E) lead to phase-modulated encoding. The excitation block is followed by a mixing period (similar to the one used in conventional 2D NMR) and by the usual EPI-based detection block.

The first amplitude-modulated encoding scheme (Fig. 1A) was proposed by Shrot et al. [21]. It is formed by a 90° continuous excitation performed by a chirp pulse with a linear frequency ramp applied during a positive gradient G_e, immediately followed by an identical 90° storage pulse applied in the presence of an opposite gradient. This second chirp pulse compensates for the quadratic z^2 phase dependence induced by the first pulse, and it stores the coherences back into longitudinal spin states. The following mixing period must flip back the magnetizations in the transverse plane before detection. However, the spatial encoding achieved by this scheme is performed from one end of the sample to the other, which can lead to a number of artefacts [19]. To compensate for these drawbacks, a symmetric amplitude-encoding scheme has been proposed by Shapira et al. [19] (Fig. 1B). It is identical to the previous one, except that both halves of the sample are swept simultaneously from the edges of the sample to the centre during the excitation pulse and vice versa during the storage pulse. The amplitude modulation involved in these two excitation schemes is incompatible with phase-modulated techniques such as COSY [1] or J-resolved spectroscopy [26]. Furthermore, these amplitude modulated schemes theoretically induce a factor of 2 loss in comparison to phase modulation. Fortunately, three different alternatives have been proposed to obtain phase-modulated encoding in order to circumvent these limitations. Tal et al.'s encoding scheme [22] (Fig. 1C) consists of a 90° continuous excitation performed by a chirp pulse identical to the one used in the amplitude-modulated scheme, applied during a G_e gradient. Then, the quadratic phase dependence is compensated by a 180° chirp pulse applied during a second gradient, whose sign can be chosen either positive or negative. We showed recently [17] that the excitation scheme using a negative gradient led to a better compromise between sensitivity and resolution than its positive counterpart. For simplicity reasons, we shall consider here the case in which the gradients have opposite amplitudes, which implies the relation $\delta^{\pi/2} = 2 \cdot \delta^{\pi}$ between pulse durations [17,22] in order to compensate for the quadratic phase dependence. Moreover, a positive gradient of identical amplitude and of duration δ^{π} must be added at the end of the excitation process for the pulse sequence to be gradient neutral.

A constant-time (CT) version of phase-modulated excitation was proposed by Pelupessy [18]. This double spin echo method (Fig. 1D) starts with a 90° non-selective pulse, followed by a pair of identical 180° chirp pulses applied during alternating gradients. The main feature of this experiment is the identical duration spent by magnetizations in the transverse plane, which does not depend on their position along the z-axis. Finally, we proposed a multi-echo derivation of the CT excitation scheme [17] (Fig. 1E) that was initially designed to compensate for molecular diffusion effects. In this pulse sequence, which is also a constant-time experiment, the two 180° chirp pulses are replaced by a succession of shorter 180° pulse pairs applied during alternated gradients.

2.2. Theoretical description of diffusion effects during the encoding process

A detailed theoretical description of molecular diffusion losses in the course of the ultrafast excitation process was given by Shrot

and Frydman in Ref. [25]. The authors demonstrated an almost perfect adequacy between analytical derivations of their model and numerical simulations. However, a minor deviation was observed between the analytical model and the experimental results in the case of the CT phase modulated excitation [25]. Therefore, we chose to proceed to numerical simulations in order to compare signal losses and line shape modifications with experimental results for all continuous encoding excitation schemes.

Before modelizing diffusion effects during the ultrafast encoding process, it should be noticed that all excitation schemes should be compared with identical T_e values so that they have the same dependence on transverse relaxation. Moreover, this comparison should be performed with identical gradient amplitudes.

Transverse diffusion effects in the presence of magnetic field gradients are quite easy to understand if we consider the resolution of Bloch equations with diffusion terms described by Torrey [27]. When a magnetic field gradient G is applied during a time t along the z-axis, the resulting signal S can be calculated by:

$$S = S_0 \exp(-i\gamma G z t) \exp\left(-\frac{1}{3} D\gamma^2 G^2 t^3\right) \tag{1}$$

where S_0 is the signal intensity before the gradient and D the transverse diffusion coefficient. When n gradients G_j are applied successively with various durations t_j, the resulting signal S_n can be obtained by applying Eq. (1) n times successively:

$$S_n = S_0 \prod_{j=1}^{n} \exp(-i\gamma G_j z t_j) \exp\left(-\frac{1}{3} D\gamma^2 G_j^2 t_j^3\right) \tag{2}$$

In the case of ultrafast excitation schemes, it is also necessary to account for successive 90° excitation or 180° inversion effects. Consequently, each excitation scheme should be divided in several successive blocks. As an example, a detailed calculation for the CT phase-modulated scheme can be found in Ref. [24]. In the present paper, this calculation is generalized to the various encoding schemes described in Fig. 1. Each one is indexed by a letter corresponding to its location in Fig. 1. For a given encoding scheme u, the decomposition into successive gradients depends on the instant τ_u when the first chirp pulse addresses an internal chemical shift Ω_1 at a particular position z. For all encoding schemes, this instant is obtained by the expression:

$$\tau_u = \frac{\Omega_1 - \xi_u O_i + \gamma_e G_e z}{\xi_u R} \tag{3}$$

with

$$\begin{cases} \xi_u = 1 & \text{for } u = a, c, d, e \\ \xi_u = -z/|z| & \text{for } u = b \end{cases} \tag{4}$$

In Eq. (3), O_i is the initial frequency offset of the first chirp pulse (90° or 180°, depending on the scheme) characterized by a sweep rate R. The parameter ξ_u (Eq. (4)) is not the same for the symmetric encoding scheme as for the other excitation patterns, as the instant τ_b depends on the sign of z, because of the symmetric sweep imparted by the chirp pulses.

Starting from these expressions, we calculated, for each encoding scheme, the remaining signal S_u at the end of the excitation process, given by the following expression:

$$S_u = S_0 \exp(-b_u D) \tag{5}$$

where b_u is a parameter depending on the instant τ_u:

$$b_u = \frac{\gamma^2 G_e^2}{3} f_u(\tau_u) \tag{6}$$

Table 1
$f_u(\tau_u)$ functions characterizing diffusion losses in continuous-encoding ultrafast excitation

u	Encoding scheme	$f_u(\tau_u)$
a	Amplitude-modulated	$2(\delta^{\pi/2} - \tau_a)^3$
b	Symmetric amplitude-modulated	$2(\delta^{\pi/2} - \tau_b)^3$
c	Phase-modulated	$(\delta^{\pi/2} - \tau_c)^3 + \left(\frac{\delta^{\pi/2}}{2} - \frac{\tau_c}{2}\right)^3 + \left(\frac{\tau_c}{2}\right)^3 + \left(\frac{\delta^{\pi/2}}{2}\right)^3$
d	CT phase-modulated	$2((\delta^{\pi} - \tau_d)^3 + (\tau_d)^3)$
e	Multi-echo	$2n((\delta^{\pi} - \tau_e)^3 + (\tau_e)^3)$

τ_u represents the instant when the first chirp pulse addresses an internal chemical shift Ω_1 at a particular position z. Pulse durations $\delta^{\pi/2}$ and δ^{π} refer to Fig. 1. $2n$ is the number of echoes for the multi-echo encoding scheme.

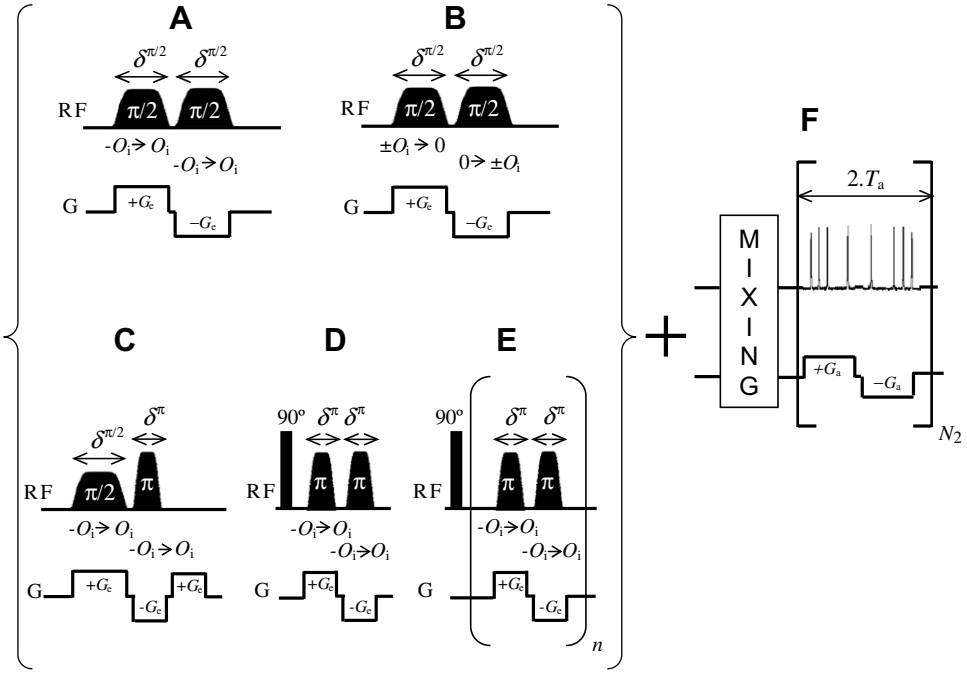

Fig. 1. Pulse sequences for the acquisition of ultrafast 2D NMR spectra, showing the different continuous encoding schemes available to perform spatially selective excitation. (A) Amplitude-modulated excitation. (B) Amplitude-modulated symmetric excitation. (C) Phase-modulated excitation. (D) Phase-modulated constant time excitation. (E) Multi-echo phase-modulated excitation. (F) Common mixing and detection periods, to be applied after any spatial encoding period.

where $f_u(\tau_u)$ is a function which fully characterizes intensity losses due to diffusion; the various expressions for $f_u(\tau_u)$ are given in Table 1. $f_u(\tau_u)$ depends on the instant τ_u defined above and on the pulse durations indicated in Fig. 1. Gradient decay and build-up times are not considered in this model, as they are very short compared to chirp pulse durations.

3. Results and discussion

3.1. Derivations and simulations

Starting from the expressions derived in Section 2.2, we calculated the signal losses due to diffusion effects for various z coordinates, for a given chemical shift Ω_1. We performed simulations for each encoding scheme, for different T_e values. In all the simulations described, the frequency range of the chirp pulses is assumed to match the one induced by the gradients. The results are presented in Fig. 2 for a diffusion coefficient $D = 2.3 \times 10^{-9}\ m^2\ s^{-1}$ corresponding to the experimental value for a pure water sample (see Section 5). It can be observed that diffusion losses highly depend on the position z. Moreover, the comparison between Fig. 2A and B shows that these losses increase with T_e. Finally, they highly depend on the encoding scheme for a given T_e value. Whereas the simple amplitude- and phase-modulated excitation schemes are characterized by asymmetric diffusion profiles, the symmetric amplitude-encoding scheme and the CT and multi-echo phase-encoding schemes lead to symmetric diffusion profiles. Simulations are shown for $\Omega_1 = 0$ but it has been shown that the intensity profile does not vary significantly over the usual ^1H chemical shift range [24].

Starting from these results, we simulated the echoes obtained when applying a detection gradient G_a immediately after excitation. As the evolution during the EPI-based detection block is similar to a conventional 2D NMR evolution, we will focus on the echo observed during the first acquisition gradient. Echo line shape simulations were carried out numerically by partitioning the sample into a large number of slices in order to approximate the continuous excitation case. The resulting signal can be described as the sum of contributions arising from the spin packets at different positions z. In our case, these contributions take into account the diffusion losses profile calculated for each excitation scheme. Shrot and Frydman have shown [28] that such a numerical simulation gave the same results as the analytical derivation of line shapes.

We simulated ultrafast echo line shapes for each excitation scheme and for two different values of T_e (Fig. 3). Transverse relaxation was not considered in this model, as all the excitation schemes are compared with identical T_e values. The echoes observed during the first acquisition gradient are represented in magnitude mode to get closer to real ultrafast processing conditions. Relative intensities are not considered in Fig. 3 but are plotted in Fig. 4. For short T_e values (30 ms), the diffusion effects are negligible and the simulated echo line shapes have the expected sinc forms already observed in ultrafast experiments [28,29]. These line shapes are almost identical for all encoding schemes. On the contrary, different behaviours are observed when T_e increases. For excitation schemes with symmetric diffusion losses (amplitude-modulated symmetric encoding, CT phase-modulated encoding and multi-echo encoding), the spins located on the edges of the sample become more affected by diffusion effects than the ones situated in the centre. Their contribution to the overall signal decreases, which leads to an attenuation of lateral sinc lobes and to significant line broadening. The latter is more important for the amplitude-modulated symmetric encoding than for the other schemes. Moreover, it can be observed that diffusion effects on echo line shapes are considerably reduced when multi-echo encoding is applied, especially when a high number of echoes are used. In this case, the line shape remains almost identical to the one observed for a short T_e value. On the contrary, for encoding schemes with asymmetric diffusion losses (simple amplitude- and phase-modulated encoding), the maximum signal at the end of the excitation process is obtained for $z \neq 0$. The consequence on line shapes is an increased contribution of lateral sinc lobes when T_e increases. Consequently, asymmetric excitation schemes appear more sensitive to diffusion effects on echo line shapes when T_e increases.

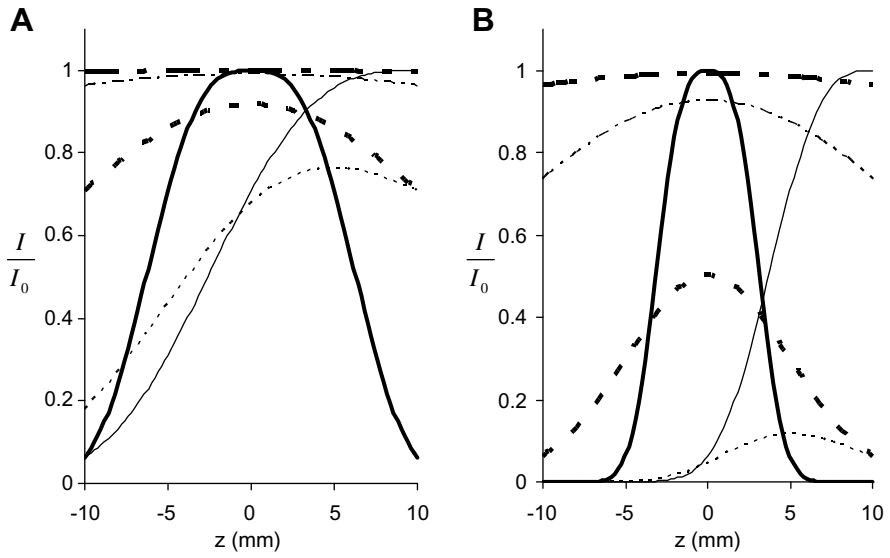

Fig. 2. Simulation of signal losses due to diffusion during excitation, for ultrafast spectra acquired with $T_e = 60$ ms (A) and $T_e = 120$ ms (B), for a diffusion coefficient $D = 2.3 \times 10^{-9}\ m^2\ s^{-1}$. — Amplitude-modulated encoding. ▬▬ Amplitude-modulated symmetric encoding. ----- Phase-modulated encoding. ▪ ▬ ▪ Constant-time phase-modulated encoding. –·– Multi-echo encoding (six echoes). ▬ ▬ ▬ Multi-echo encoding (12 echoes). Curves obtained for $\Omega_1 = 0$ are represented, but simulations performed at different frequencies show that diffusion losses do not vary significantly over the ^1H chemical shift range. Transverse relaxation was not considered in this model.

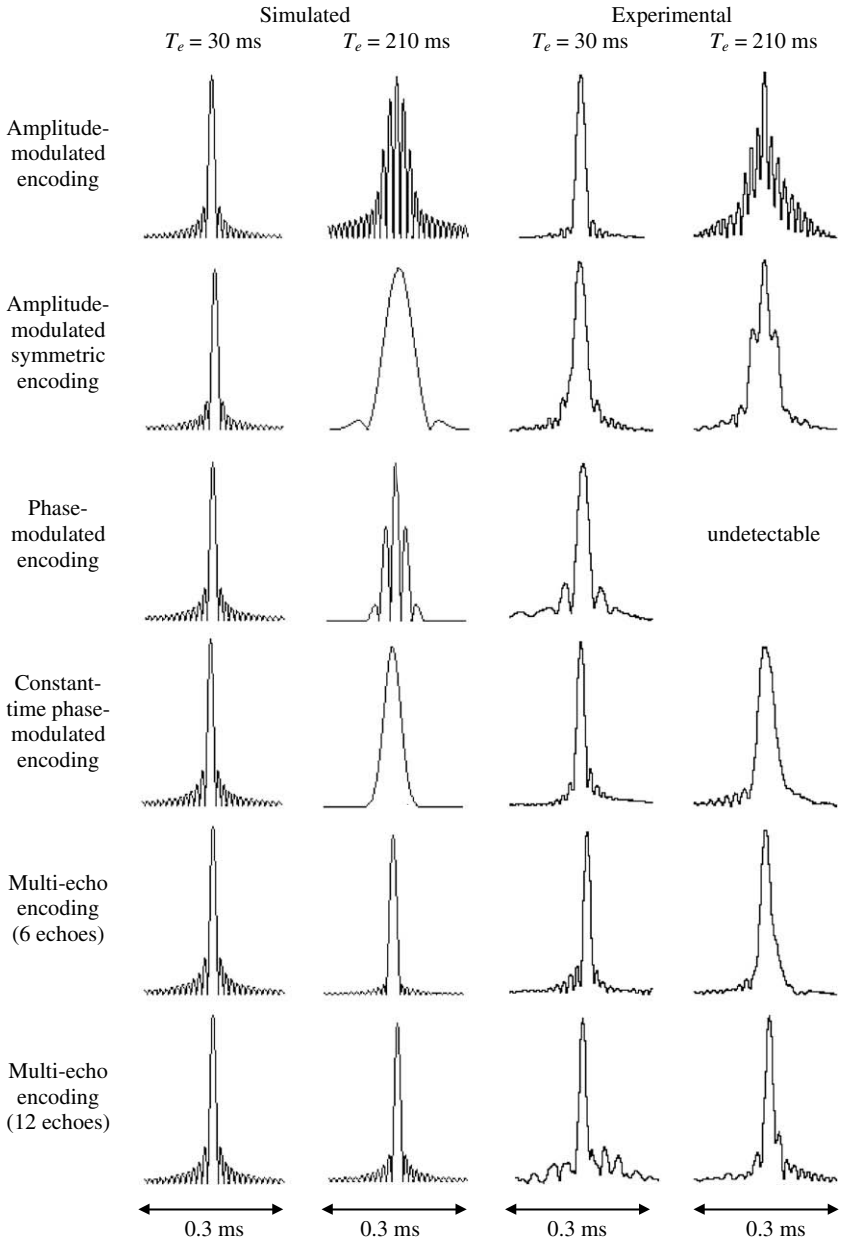

Fig. 3. Simulated and experimental echoes obtained during the first acquisition gradient of ultrafast experiments performed with different encoding schemes and different T_e values. Simulations performed at zero frequency with $D = 2.3 \times 10^{-9}$ m^2 s^{-1}. Experiments performed at 298 K for a water sample. The excitation frequency was set on the water signal. Gradient parameters are indicated in Section 5.

It is also interesting to plot the ultrafast echo intensity as a function of T_e, which determines the intensity decrease for 2D peaks. This evolution is plotted in Fig. 4A for the various excitation schemes. Signal losses due to diffusion effects when T_e increases can be observed for all the encoding schemes. It is interesting to notice that similar curves are obtained for both amplitude-modulated encoding schemes. They appear less sensitive to intensity losses than the simple phase-modulated scheme for any T_e, and than the CT phase-modulated scheme for high T_e values only. Finally, one can observe that the multi-echo scheme appears far less sensitive to diffusion losses, and that it is all the more efficient since the number of echoes is high.

For comparison, we also plotted (Fig. 4B) the simulated losses for a smaller coefficient diffusion (10^{-10} m^2 s^{-1}) corresponding to protein-type conditions [25]. As expected, for all encoding schemes, the signal losses are reduced compared to the small molecule conditions. However, the relative sensitivity of the various excitation schemes to diffusion losses remains qualitatively the same.

In this part, we have discussed molecular diffusion effects during the excitation process. It could also be interesting to consider possible diffusion losses during the acquisition period. As alternative gradients are applied during the detection process, it could a priori lead to diffusion losses as well as during the acquisition period. However, most ultrafast pulse sequences require short acquisition gradients (typically a few hundreds of microseconds), and it was recently highlighted [24,25] that diffusion effects during acquisition period were negligible in this case. The effects of diffusion on line shape simulated here may also be cumulated with possible effects depending on the mixing period. However, these effects were not discussed here because the mixing period is identical for the different experiments.

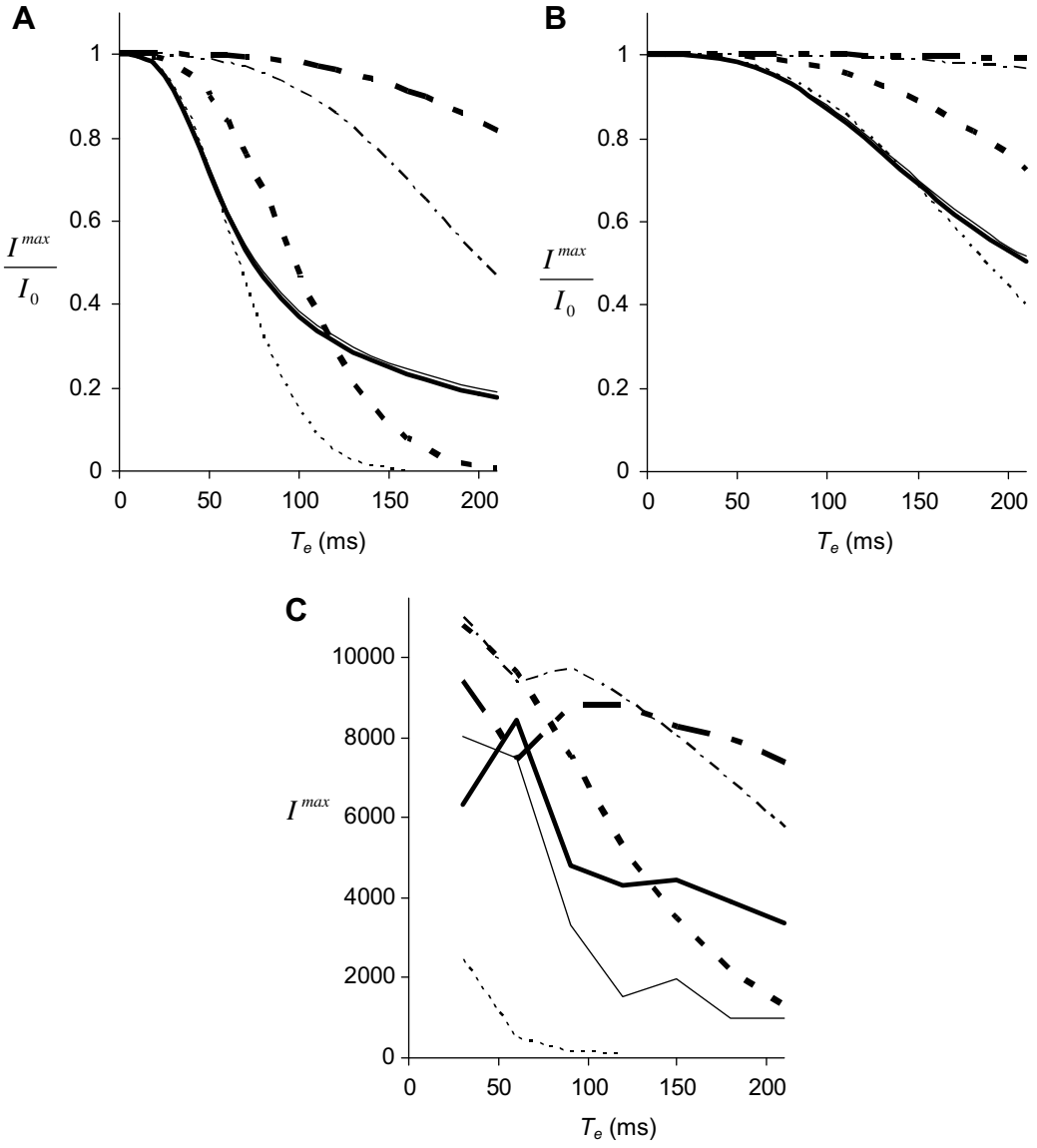

Fig. 4. (A) Simulated signal losses due to diffusion during excitation for a diffusion coefficient $D = 2.3 \times 10^{-9}$ m^2 s^{-1} and (B) for $D = 10^{-10}$ m^2 s^{-1}. The curves obtained for $\Omega_1 = 0$ are represented, but simulations performed at different frequencies show that diffusion losses do not vary significantly over the ^{1}H chemical shift range. Transverse relaxation was not considered in this model. (B) Experimental signal losses for a pure water sample at 298 K. The excitation frequency was set on the water signal. Gradient parameters are indicated in Section 5. Average intensities were measured from five consecutive experiments. Arbitrary vertical scale. — Amplitude-modulated encoding. ▬▬ Amplitude-modulated symmetric encoding. ----- Phase-modulated encoding. ▬ ▬ ▪ Constant-time phase-modulated encoding. –·– Multi-echo encoding (six echoes). ▬ ▪ ▬ Multi-echo encoding (12 echoes).

3.2. Experimental observations

In order to compare the theoretical results presented above with experimental observations, we performed ultrafast experiments on a water sample characterized by a diffusion coefficient $D = 2.3 \times 10^{-9}$ m^2 s^{-1} at 25 °C. The experimental line shapes obtained for the various encoding schemes are represented in Fig. 3, together with the simulated echoes. A good qualitative adequacy between theoretical and experimental results is observed. In particular, line broadening clearly appears when T_e increases, and one can notice that it is far less important when the multi-echo scheme is employed, which confirms the low sensitivity of this scheme to diffusion effects. In particular, the line shape is almost unaffected when 12 echoes are employed. Also noticeable is the increasing contribution of lateral sinc lobes for the simple amplitude-modulated encoding scheme. The line shape obtained for $T_e = 210$ ms is very similar to the simulated one.

However, a number of differences between simulated and experimental line shapes can be noticed. For the amplitude-modulated symmetric scheme, line shape distortions can be observed. They are probably due to an imperfect excitation in the centre of the sample that was not considered in the simulations. For the simple phase-modulated scheme, lateral sinc lobe distortions can be observed at $T_e = 30$ ms. Moreover, we were not able to detect any signal for $T_e = 210$ ms. Actually, this encoding scheme is the most sensitive to diffusion effects (see Fig. 4), and the theoretical signal remaining after a 210 ms excitation is only $2 \times 10^{-6} S_0$, which explains that the echo was not detected. Finally, for the multi-echo scheme, artefacts at the base of the peaks can be observed for short T_e (30 ms) and a high number of echoes ($2 \cdot n = 12$). These artefacts may be due to adiabaticity losses when 180° pulse durations become too short, since the adiabaticity factor is directly proportional to pulse duration [30]. When the same frequency width is swept in a shorter duration, the inversion becomes less efficient. For this

reason, the number of echoes cannot be increased indefinitely, especially for short T_e values.

We plotted the experimental intensity losses for each encoding scheme in Fig. 4C. The intensity losses observed experimentally are similar to the theoretical curves from a qualitative point of view. The adequacy between simulated and experimental evolutions validates our theoretical model, confirming the importance of diffusion effects for slow-relaxing molecules such as water. As expected by the theory, the simple phase-modulated scheme is the most sensitive to diffusion losses, which explains that no signal could be detected for T_e higher than 120 ms. However, the signal detected for this encoding scheme is unexpectedly weak compared to the other curves. This is due to additional losses which probably originate from pulse imperfections (see Section 3.3). Such imperfections also explain the important losses observed at short T_e for the amplitude modulated symmetric excitation, because of the peculiar nature of the double-sweep pulses applied in this case.

The most important feature in Fig. 4C is the efficiency of the multi-echo scheme, which is far less sensitive to diffusion than the other schemes. The influence of the number of echoes is clearly visible for high T_e values. However, for this encoding scheme, intensities observed at T_e = 60 ms are unexpectedly low, probably because of the artefacts and distortions observed when short adiabatic pulses are employed. Finally, for short T_e values, simple amplitude modulated and CT phase-modulated schemes appear to give the best results.

3.3. Discussion

In the light of the theoretical and experimental results presented above, it is now possible to determine the optimum encoding scheme to perform ultrafast excitation with a good resolution (i.e. with high T_e values) while minimizing intensity losses. The choice depends on whether one is interested in amplitude- or phase-modulated encoding. Moreover, the choice of T_e depends on the desired resolution and may also be restrained to a small value for large spectral widths. For short T_e values, optimum results in terms of intensity and echo line shape are obtained using either the simple amplitude-modulated encoding scheme or the constant-time phase-modulated encoding pattern. The choice between these two schemes will then depend on the kind of modulation desired. For short T_e values, the symmetric amplitude-encoding and the multi-echo scheme should be avoided because they give rise to artefacts at the base of the peaks. For long T_e values, the multi-echo excitation scheme should be preferred to other schemes, because it is far less sensitive to diffusion effects on echo line shape and intensity. Finally, for all T_e values, the simple phase-encoding scheme should be avoided because intensity losses due to diffusion are much higher than with other schemes.

It is also interesting to say a few words on the robustness of the various encoding sequences. When setting the different excitation schemes, it appeared that they did not have the same sensitivity to experimental parameter variations, such as pulse power or frequency offset. In particular, the simple phase-encoding excitation scheme seems very sensitive to these effects. Moreover, important artefacts are observed even for short T_e values. This may be due to the asymmetry of the pulse sequence: because the two successive 90° and 180° pulses are not identical or symmetric, their imperfections may not mutually compensate, contrary to other excitation schemes. And, we also observed that encoding schemes including 90° chirp pulses were less robust than other schemes to pulse parameter variations. On the contrary, for encoding schemes employing 180° chirp pulses only (constant-time and multi-echo phase encoding), the echo line shape and intensity appear very robust to small parameter variations. The main cause is probably the need for 90° chirp pulses to have a precise adiabaticity factor value (α = 0.068) [31] to perform an efficient excitation, whereas 180° chirp pulses are efficient in a wide range of adiabaticity factors.

The pulse imperfections may also explain the additional line broadening that can be clearly observed in Fig. 3. For all the excitation schemes, the experimental half-height width, $\Delta\upsilon_{exp}^{1/2}$ is somewhat higher than the simulated one, $\Delta\upsilon_{th}^{1/2}$. This effect is probably due to an imperfect magnetization refocusing originating from pulse imperfections. However, this effect appears to be more important when the excitation scheme includes 90° chirp pulses than when only 180° pulses are employed. For example, for T_e = 30 ms, $\Delta\upsilon_{th}^{1/2} = 15$ μs whereas $\Delta\upsilon_{exp}^{1/2} = 18$ μs for the CT phase-modulated scheme and $\Delta\upsilon_{exp}^{1/2} = 21$ μs for the simple amplitude-modulated scheme. Consequently, the robustness and line-broadening effects described above may direct the choice of the encoding pattern towards the schemes formed of 180° chirp pulses only, when it is compatible with the kind of signal modulation required by the user.

It is evidence that the choice of the excitation scheme is not the only way of limiting diffusion effects during excitation. These effects all depend on G_e^2; consequently it is important to use weak gradient amplitudes, which was already the case in the experiments presented above, where G_e value was 2% of the maximum gradient strength available. However, the frequency range of the chirp pulses is assumed to match the one induced by the gradient G_e. Therefore, for weaker values of G_e, the frequency range of the chirp pulses was not large enough in comparison to the chemical shift range. That probably explains why baseline distortions were observed when G_e was decreased under 2%. Finally, another possibility is to limit the diffusion coefficient D, for example by working at low temperature and by using a viscous solvent when possible.

The last remark concerns the line shape considerations presented in this paper. It should be reminded that only the echo line shape along the ultrafast dimension was studied, and that the 2D line shapes will often be more complicated, as detailed by Shrot and Frydman [20], presenting both dispersive and absorptive components. Moreover, long mixing periods may also cause diffusion losses as noticed in Section 3.1.

4. Conclusion

This paper highlights the important role of molecular diffusion effects in ultrafast 2D NMR experiments and shows the necessity to employ an appropriate excitation scheme to perform the spatial encoding required by this kind of experiments, particularly when one wants to obtain spectra with a good resolution along the ultrafast dimension. The experimental and theoretical results presented here permit a direct comparison between the various encoding schemes, moreover they put in evidence the efficiency of the multi-echo scheme that we have recently proposed [17].

Future developments could include a detailed optimization of the chirp pulse adiabaticity in order to limit artefacts at the base of the peaks and to optimize the efficiency of the excitation process, in particular when short adiabatic pulses are employed.

The optimization of the sensitivity/resolution compromise presented in this paper opens interesting perspectives in numerous domains of magnetic resonance. Resolution improvements could progressively lead to the replacement of conventional 2D NMR by ultrafast methods in a wide range of applications, from structure elucidation to biomolecular NMR or in vivo spectroscopy. The new improvements presented here could also be useful for quantitative applications, where the reduction of experiment duration plays a central role [32]. Despite the improvements discussed above, ultrafast nD NMR is still limited by a low sensitivity inherent to the method itself, as recently noticed by Frydman [33]. Consequently, ultrafast methods can be used only when sufficient

signal-to-noise ratio is available, which makes the method unsuitable for low-concentrated samples. Future investigations will consider the use of ultrafast nD experiments together with dynamic nuclear polarization (DNP) [34], in order to reduce the detection limit by several orders of magnitude.

5. Experimental

Experiments were performed on a water sample (including 20% D_2O as a lock substance) analyzed in a 5 mm tube and characterized by a diffusion coefficient $D = 2.3 \times 10^{-9}\ m^2\ s^{-1}$. NMR spectra were recorded at 298 K on a Bruker Avance 500 DRX spectrometer, at a frequency of 500.13 MHz with a triple resonance TBI probe including z-axis gradient. All experiments were performed with Wurst-100 encoding pulses [35] with a sweep range of 9.4 kHz, applied during $G_e = 0.011\ T\ m^{-1}$ excitation gradients. Pulse durations were adapted to reach the desired T_e value. The acquisition gradient G_a was set to $0.097\ T\ m^{-1}$. The excitation frequency was set on the water signal. No mixing period was applied for simplicity reasons.

All spectra were acquired and analysed using the Bruker program Topspin 2.0. The specific processing for ultrafast spectra was performed using our home-written routine in Topspin.

Simulations were carried out using a home-written program in Matlab, using the same excitation and detection parameters as the experimental values.

Acknowledgment

The authors thank Michel Giraudeau for efficient linguistic assistance.

References

[1] W.P. Aue, E. Bartholdi, R.R. Ernst, Two-dimensional spectroscopy: application to nuclear magnetic resonance, J. Chem. Phys. 64 (1976) 2229–2246.
[2] J. Jeener, Lecture presented at Ampere International Summer School II, Basko Polje, Yugoslavia, September 1971.
[3] A.F. Mehlkopf, D. Korbee, T.A. Tiggelman, R. Freeman, Sources of t_1 noise in two-dimensional NMR, J. Magn. Reson. 58 (1984) 315–323.
[4] P. Schanda, B. Brutscher, Very fast two-dimensional NMR spectroscopy for real-time investigation of dynamic events in proteins on the time scale of seconds, J. Am. Chem. Soc. 127 (2005) 8014–8015.
[5] H. Barkhuijsen, R. De Beer, W.M.M.J. Bovée, D. Van Ormondt, Retrieval of frequencies, amplitudes, damping factors, and phases from time-domain signals using a linear least-squares procedure, J. Magn. Reson. 61 (1985) 465–481.
[6] A.S. Stern, K.-B. Li, J.C. Hoch, Modern spectrum analysis in multidimensional NMR spectroscopy: comparison of linear-prediction extrapolation and maximum-entropy reconstruction, J. Am. Chem. Soc. 124 (2002) 1982–1993.
[7] J.C. Hoch, Maximum entropy signal processing of two-dimensional NMR data, J. Magn. Reson. 64 (1985) 436–440.
[8] E. Kupce, R. Freeman, Projection–reconstruction technique for speeding up multidimensional NMR spectroscopy, J. Am. Chem. Soc. 126 (2004) 6429–6440.
[9] V.A. Mandelshtam, H.S. Taylor, A.J. Shaka, Application of the filter diagonalization method to one- and two-dimensional NMR spectra, J. Magn. Reson. 133 (1998) 304–312.
[10] E. Kupce, R. Freeman, Frequency-domain Hadamard spectroscopy, J. Magn. Reson. 162 (2003) 158–165.
[11] E. Kupce, R. Freeman, Two-dimensional Hadamard spectroscopy, J. Magn. Reson. 162 (2003) 300–310.
[12] M. Feliz, J. Garcia, E. Aragón, M. Pons, Fast 2D NMR ligand screening using Hadamard spectroscopy, J. Am. Chem. Soc. 128 (2006) 7146–7147.
[13] L. Frydman, A. Lupulescu, T. Scherf, Principles and features of single-scan two-dimensional NMR spectroscopy, J. Am. Chem. Soc. 125 (2003) 9204–9217.
[14] L. Frydman, T. Scherf, A. Lupulescu, The acquisition of multidimensional NMR spectra within a single scan, Proc. Natl. Acad. Sci. USA 99 (2002) 15858–15862.
[15] P. Mansfield, Spatial mapping of the chemical shift in NMR, Magn. Reson. Med. 1 (1984) 370–386.
[16] Y. Shrot, L. Frydman, Ghost-peak suppression in ultrafast two-dimensional NMR spectroscopy, J. Magn. Reson. 164 (2003) 351–357.
[17] P. Giraudeau, S. Akoka, Resolution and sensitivity aspects of ultrafast J-resolved 2D NMR spectra, J. Magn. Reson. 190 (2008) 339–345.
[18] P. Pelupessy, Adiabatic single scan two-dimensional NMR spectroscopy, J. Am. Chem. Soc. 125 (2003) 12345–12350.
[19] B. Shapira, Y. Shrot, L. Frydman, Symmetric spatial encoding in ultrafast 2D NMR spectroscopy, J. Magn. Reson. 178 (2006) 33–41.
[20] Y. Shrot, L. Frydman, Spatial encoding strategies for ultrafast multidimensional nuclear magnetic resonance, J. Chem. Phys. 128 (2008) 052209.
[21] Y. Shrot, B. Shapira, L. Frydman, Ultrafast 2D NMR spectroscopy using a continuous spatial encoding of the spin interactions, J. Magn. Reson. 171 (2004) 163–170.
[22] A. Tal, B. Shapira, L. Frydman, A continuous phase-modulated approach to spatial encoding in ultrafast 2D NMR spectroscopy, J. Magn. Reson. 176 (2005) 107–114.
[23] P. Giraudeau, S. Akoka, A new detection scheme for ultrafast J-resolved spectroscopy, J. Magn. Reson. 186 (2007) 352–357.
[24] P. Giraudeau, S. Akoka, Sources of sensitivity losses in ultrafast 2D NMR, J. Magn. Reson. 192 (2008) 151–158.
[25] Y. Shrot, L. Frydman, The effects of molecular diffusion in ultrafast two-dimensional nuclear magnetic resonance, J. Chem. Phys. 128 (2008) 164513.
[26] W.P. Aue, J. Karhan, R.R. Ernst, Homonuclear broad band decoupling and two-dimensional J-resolved NMR spectroscopy, J. Chem. Phys. 64 (1976) 4226–4227.
[27] H.C. Torrey, Bloch equations with diffusion terms, Phys. Rev. 104 (1956) 563–565.
[28] Y. Shrot, L. Frydman, Single-scan NMR spectroscopy at arbitrary dimensions, J. Am. Chem. Soc. 125 (2003) 11385–11396.
[29] B. Shapira, A. Lupulescu, Y. Shrot, L. Frydman, Line shape considerations in ultrafast NMR, J. Magn. Reson. 166 (2004) 152–163.
[30] E. Tenailleau, S. Akoka, Adiabatic ^1H decoupling scheme for very accurate intensity measurements in ^{13}C NMR, J. Magn. Reson. 185 (2007) 50–58.
[31] Y. Shrot, L. Frydman, Spatially encoded NMR and the acquisition of 2D magnetic resonance images within a single scan, J. Magn. Reson. 172 (2005) 179–190.
[32] P. Giraudeau, N. Guignard, H. Hillion, E. Baguet, S. Akoka, Optimization of homonuclear 2D NMR for fast quantitative analysis: application to tropine–nortropine mixtures, J. Pharmaceut. Biomed. Anal. 43 (2007) 1243–1248.
[33] L. Frydman, Single-scan multidimensional NMR, C.R. Chimie 9 (2006) 336–345.
[34] L. Frydman, D. Blazina, Ultrafast two-dimensional nuclear magnetic resonance spectroscopy of hyperpolarized solutions, Nat. Phys. 3 (2007) 415–419.
[35] E. Kupce, R. Freeman, Adiabatic pulses for wideband inversion and broadband decoupling, J. Magn. Reson. A 115 (1995) 273–276.